buildings

MDPI

Article

Analysis of Seismic Performance and Applicable Height of a Cooperative Modular Steel Building

Yan Wang, Zhuyu Huang and Qi An *

School of Civil Engineering, Qingdao University of Technology, Qingdao 266520, China; yanwang2010803@163.com (Y.W.); 17866828258@163.com (Z.H.)
* Correspondence: anqi@qut.edu.cn

Abstract: As an innovative building system, the modular steel structure demonstrates a high degree of industrialization and assembly efficiency. However, no linkage exists between the components of modular units, leading to issues such as diminished load capacity and excessive steel usage in modular construction. In order to tackle these challenges, finite element numerical simulations are employed to examine the inter-column connectors and the cooperative modular steel buildings. This simulation calculates the initial stiffness across various degrees of freedom in these connectors. In addition, it analyzes the displacement response, changes in internal forces, and height of cooperative modular steel structures under varying seismic precautionary intensities. The results revealed that cooperative modular steel buildings substantially improve overall stiffness and lateral performance compared to their non-cooperative counterparts. There is a maximum reduction in the inter-story displacement angle of up to 36.1%, and the maximum reduction of the top displacement can reach 16.2%. This enhancement also increases structural stiffness, a shortened natural vibration period, and an augmented bottom shear force. Based on these findings, it is advised that the height of cooperative modular steel buildings should not exceed 21 m at 7 degrees (0.10 g), 21 m at 7 degrees (0.15 g), and 12 m at 8 degrees (0.20 g).

Keywords: modular steel building; self-locking; inter-column connector; seismic performance; applicable height

check for updates

Citation: Wang, Y.; Huang, Z.; An, Q. Analysis of Seismic Performance and Applicable Height of a Cooperative Modular Steel Building. *Buildings* **2024**, *14*, 678. https://doi.org/10.3390/buildings14030678

Academic Editor: Daniele Perrone

Received: 23 December 2023
Revised: 17 January 2024
Accepted: 27 February 2024
Published: 4 March 2024

1. Introduction

In the context of China's vigorous promotion of building industrialization, along with industrial transformation and upgrading, prefabricated buildings are undergoing new upgrades. As an emerging form of prefabricated construction, modular building boasts high industrialization, superior engineering quality, and rapid construction speed. Existing modular steel buildings typically achieve module connections through corner connection nodes. Scholars worldwide have devised various corner connection nodes, analyzing their mechanical properties to ensure reliable connections between modular units [1–3]. Lawson et al. [4] designed a single bolted connector, welding a joint plate at the module column's end, setting construction holes simultaneously, and using high-strength bolts to unite the upper and lower modules. This joint, constructed outside the structure, does not interfere with interior decoration, but hole openings reduce the column end's stiffness. Liu et al. [5] introduced a new modular inner sleeve connection node, facilitating horizontal and vertical connections between modules. However, this node requires welding, increasing the on-site workload and hindering assembly construction. Chen et al. [6] proposed a self-locking inter-module connection based on a locking concept, preserving modular units' integrity and interior decoration. They indicated that this node exhibits excellent hysteresis performance and moment transfer capabilities, but its multiple mechanical components can lead to performance instability. Existing structural systems, connected by corner nodes, lack effective connections between modular unit columns. Each column operates independently, unable to form a cooperative working mode, leading to insufficient structural integrity, low load capacity, high steel consumption, and elevated costs. Hence, developing a cooperative force mode between modular units to enhance modular steel building integrity and load capacity is imperative.

Some scholars have investigated these issues. Palazzo et al. [7] suggested a novel energy-dissipating column design using X-shaped steel strips made from low-yield point steel to connect columns, thereby improving lateral resistance in horizontal directions. However, this connection requires considerable on-site work, conflicting with modular buildings' rapid construction ethos. Sharafi et al. [8] achieved a partial connection between modular unit beams using sawtooth connectors, facilitating cooperative force to some extent. As a unidirectional force transmission mode, this connector cannot support three-way force transmission and has questionable structural reliability. Yang et al. [9] explored a structural approach combining steel plate column-column and bolted beam-beam with backing plates, analyzing its seismic performance. They demonstrated significant improvements in rigidity, load capacity, and seismic performance after combining steel modular components. However, this method requires disrupting the envelope structure of modular units for assembly space. Xu et al. [10] used bolt connectors for connecting channel steel modular beams of adjacent units. They indicated that beam load capacity can increase by 50–90.5% post-combination. However, this method, necessitating the destruction of the modular units' enclosure, suits only non-closed sections. Addressing issues in existing modular steel buildings, such as poor integrity, low loading capacity, high steel usage, and cost, An et al. [11,12] proposed a self-locking inter-column connector enabling reliable connections between horizontally adjacent modules. This connector, simple in structure and requiring no extra construction space, supports rapid assembly. Under the premise of maintaining modular unit integrity, the inter-column connectors facilitate cooperative work between horizontally adjacent modular unit columns, boosting load capacity and enhancing structural integrity.

In this paper, an innovative cooperative modular steel building system is proposed based on the self-locking inter-column connector [11]. However, the stress principle of the collaborative stress modular steel structure is different from that of the conventional modular structure, and the research results of the conventional module structure cannot be directly applied to the new system. Research into the seismic mechanism and applicable height of cooperative modular steel buildings remains limited, posing challenges for engineering applications. Modular steel-structured buildings generally have problems such as small overall stiffness and poor structural displacement response in high-intensity areas. With the increase in floors, the inter-story displacement angle is also at risk of increasing. An excessive inter-story displacement angle will not only cause a large floor tilt angle and affect the normal use of the building but also cause vertical loads to have a large overturning moment on the structure, affecting structural safety. In order to overcome these challenges, this study investigates the seismic performance and applicable height of cooperative modular steel buildings through finite element analysis.

2. Cooperative Modular Steel Building System

The cooperative modular steel building, comprising modular units connected with inter-column connectors and an inner sleeve connector node [6], is depicted in Figure 1. The inter-column connector is a mortise-and-tenon structure consisting of two parts: a concave connector and a convex connector. The concave connector includes a trapezoidal chute and holes for the sliding blocks, while the convex connector comprises a trapezoidal member, a connecting backplane, a spring, and sliding blocks.

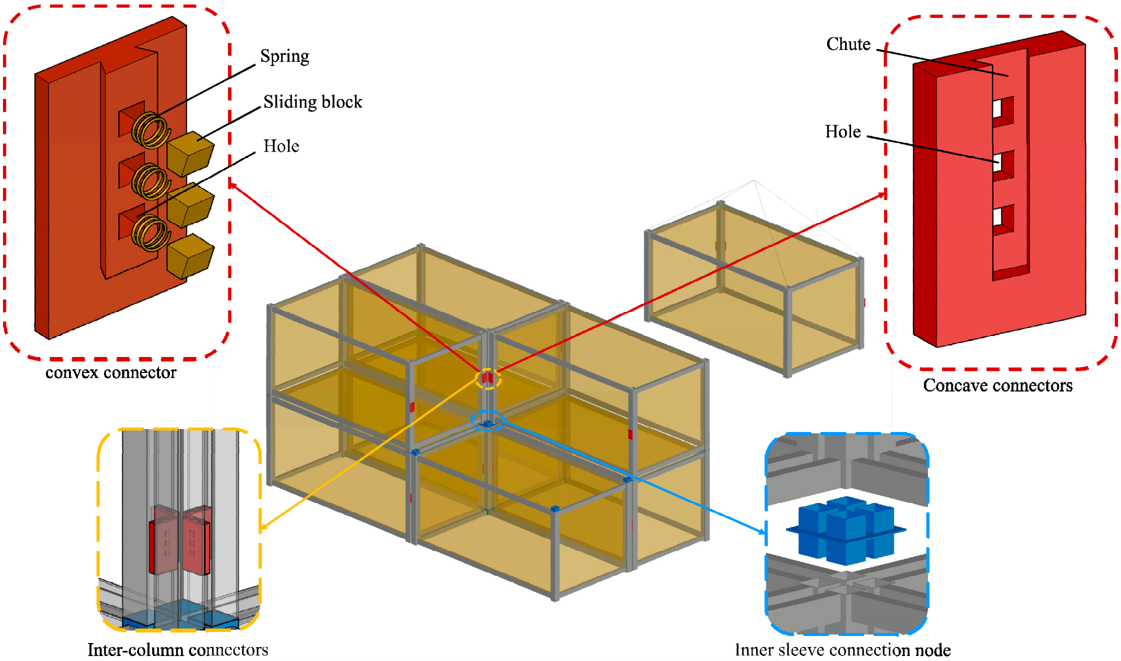

Figure 1. Cooperative modular steel building.

Figure 2 illustrates the assembly process of the inter-column connector. The concave connector is welded to modular column A, and the convex connector is welded to modular column B in the factory. At the construction site, modular unit A is hoisted into place, followed by modular unit B to the specified position, allowing the trapezoidal component of the convex connector to insert into the trapezoidal chute of the concave connector. The sliding blocks would be squeezed and then ejected during the slow descent of modular unit B. The connection is considered complete only when the lock is fully engaged and the trapezoidal member of the convex connector slides to the end of the trapezoidal chute of the concave connector. This involves the convex connector descending along the vertical direction with modular unit B until these conditions are met.

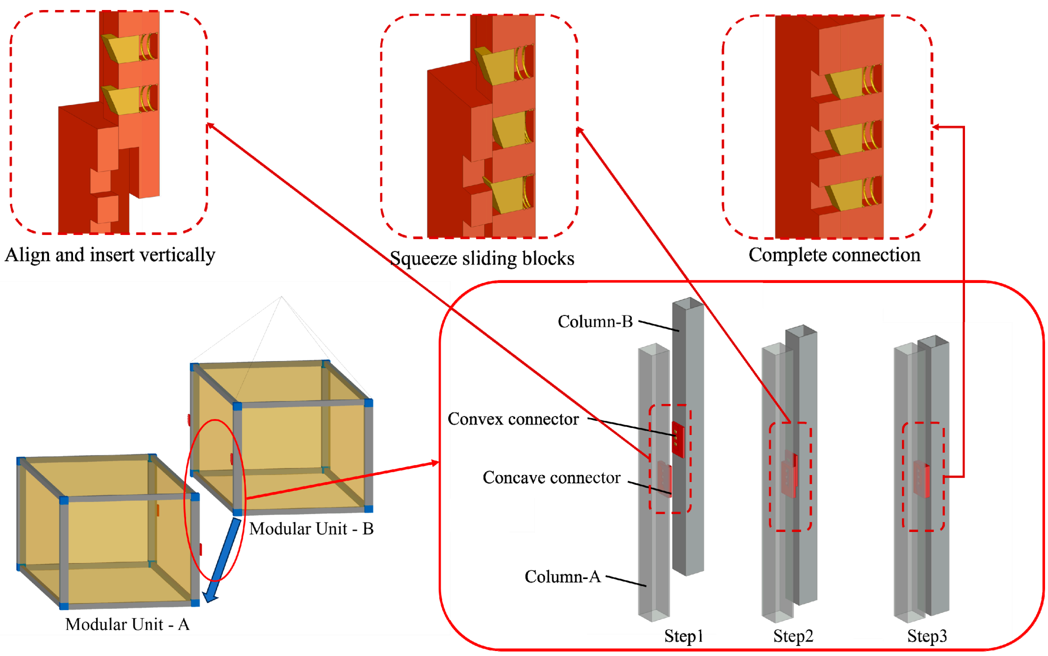

Figure 2. Connection process of the modular unit columns with an inter-column connector.

3. Initial Stiffness of the Inter-Column Connector

The inter-column connectors transfer shear force, bending moment, and axial force between the modular columns. This section investigates the initial stiffness of each degree of freedom of the inter-column connector to perform the equivalent connection of the inter-column connector in MIDAS/Gen.

3.1. Finite Element Simulation Scheme and Parameter Design

3.1.1. Element Selection and Material Constitutive Relationship

The inter-column connector is modeled and analyzed using ABAQUS. Each component in the model is assigned the element type C3D8R (eight-node linear solid element). The same force is applied to the convex connector along the Z direction, and the final displacement of the convex connector at different mesh densities is observed, as shown in Figure 3. The calculation indicates that the final displacement changes little when the mesh density is less than 1 mm. In order to ensure accuracy and convergence, the mesh size is set at 1 mm. Q355 steel is selected as the material. The material property of all components in the connector is set to be elastoplastic. Young's modulus and Poisson's ratio are assigned values of 210 GPa and 0.3, respectively. The yield strength is 355 MPa, and the ultimate strength is 470 MPa. Considering the hardening stage, the bilinear kinematic hardening model is selected as the constitutive relation, obeying the Von Mises yield criterion.

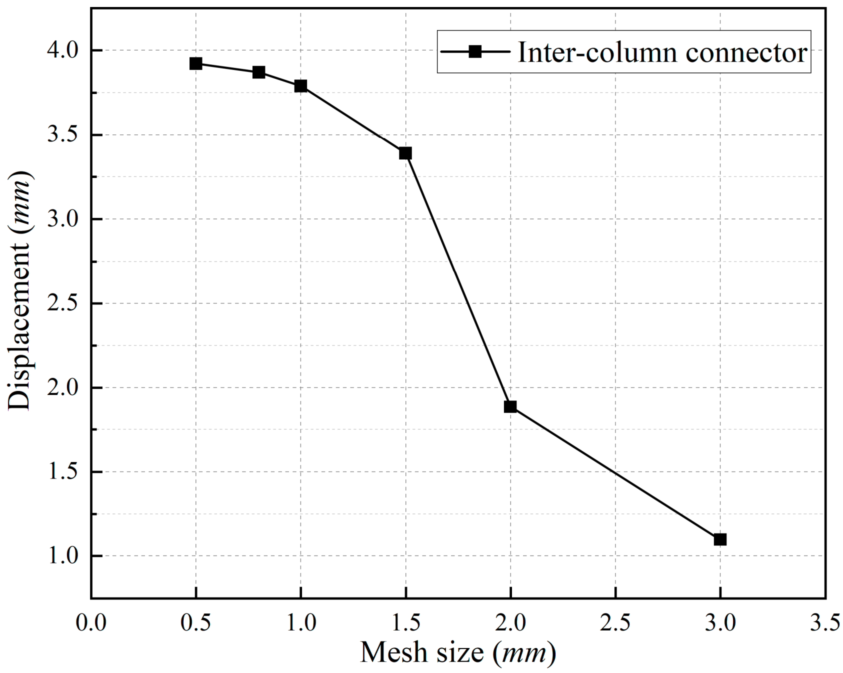

Figure 3. The change in the final displacement of the convex connector with the change in mesh density.

3.1.2. Contact Setting, Boundary Conditions, and Loading Regime

The concave and convex connectors are prepared according to the steel structure design standard (GB50017-2017) [13], including shot blasting treatment. The contact between these connectors is configured as a surface-to-surface contact. For the contact property, the contact in the normal direction is set as hard contact, while the tangential direction is established as frictional contact with a friction coefficient of 0.4. Only hard contact is made between the hole and the sliding block. The backplane of the concave connector is fixed, whereas the backplane of the convex connector releases in-plane degrees of freedom in the loading direction and applies a displacement load at the coupling point RP1 on the back of the convex connector, as shown in Figure 4.

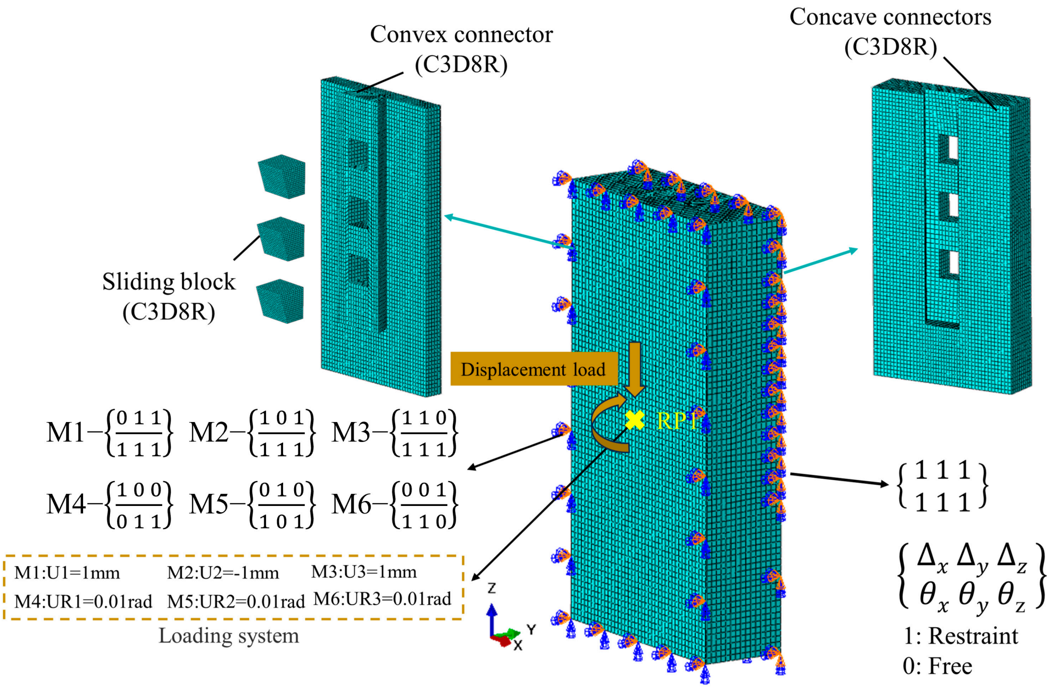

Figure 4. A finite element model of an inter-column connector.

3.1.3. Parameter Design

A total of six inter-column lateral connector models are designed, as shown in Table 1. Models M1–M3 are employed to calculate the translational stiffness of the connectors in the x, y, and z directions, respectively. Models M4–M6 determine the rotational stiffness in the Rx, Ry, and Rz directions. All numerical models are the same size, and their specific dimensions are detailed in Figure 5.

Table 1. Model parameter design.

Model Parameter	Load Direction	Load Displacement
M1	U1	1 mm
M2	U2	−1 mm
M3	U3	1 mm
M4	UR1	0.01 rad
M5	UR2	0.01 rad
M6	UR3	0.01 rad

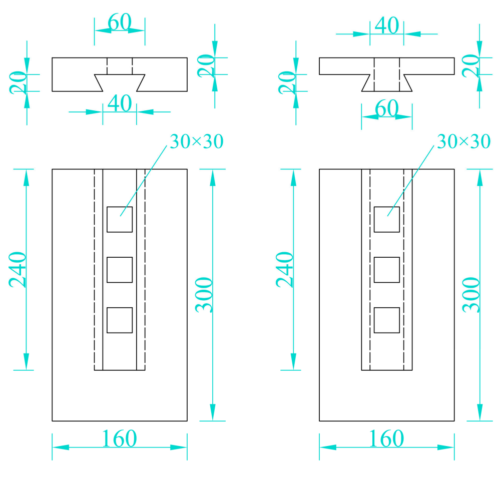

Figure 5. Dimensions of an inter-column connector.

3.2. Analysis Results

The farthest point method [14] is employed to process the data, with the initial stiffness of each degree of freedom of the inter-column connector presented in Table 2.

Table 2. The initial stiffness of each degree of freedom of the inter-column connector.

Direction of Freedom	Initial Stiffness
Dx	4309.1×10^3 kN/m
Dy	3543.5×10^3 kN/m
Dz	2556.3×10^3 kN/m
Rx	47,541.4 kN·m/rad
Ry	77,080.9 kN·m/rad
Rz	1123.8 kN·m/rad

4. Seismic Performance of a Cooperative Modular Steel Building

4.1. Seismic Fortification Intensity and Load Parameter Setting

According to the code for seismic design of buildings (GB 50011-2010) [15] and the code for load of building structures (GB 50009-2012) [16], building calculation parameters are designed and selected as follows: The structure's service life is 50 years, the safety grade is two, and the building type is class C. The seismic fortification intensity is considered between 7 and 8 degrees, with basic earthquake accelerations of 0.10, 0.15, and 0.20 g, respectively. The building falls into the second earthquake group, with a site category of class III and a characteristic period of 0.55 s. The essential wind pressure is set at 0.45 kN/m^2, the primary snow pressure at 0.15 kN/m^2, and the ground roughness at class C, considering load conditions and combinations under constant, live, wind, and earthquake loads.

4.2. Modeling Scheme and Parameter Design

4.2.1. Modeling Scheme

In this section, MIDAS/Gen is employed to model and analyze a modular steel building. In order to ensure the safety and stability of the modular steel building, the following numerical modeling methods are used: The beam-column joints of the module unit are all set as rigid joints. The connection between modular units involves extending the beam-column joints of the upper and lower parts of the module upward and downward to a short column, simulating the vertical connection of the joints. Similarly, the beam-column joints of the module extend a short beam to adjacent modular units to simulate the horizontal connections. The intersection points of the short columns are designated as rigid, as are the intersection points of the short beams, as depicted in Figure 6. Due to an uneven distribution of stiffness in the modular building, where internal stiffness is greater than peripheral stiffness, several supports are strategically placed outside the building to increase the torsional stiffness of the structure. Unlike conventional steel frame structures, which often assume a rigid floor, the modular building exhibits small gaps between units and lacks cooperative work between beams, making it imperative to consider the influence of these gaps on structural force transmission. The results have shown significant deviations between the rigid and elastic floor assumptions, as referenced in [17]. The elastic floor assumption is the preferred calculation method to accurately represent the actual forces in the modular steel frame structure.

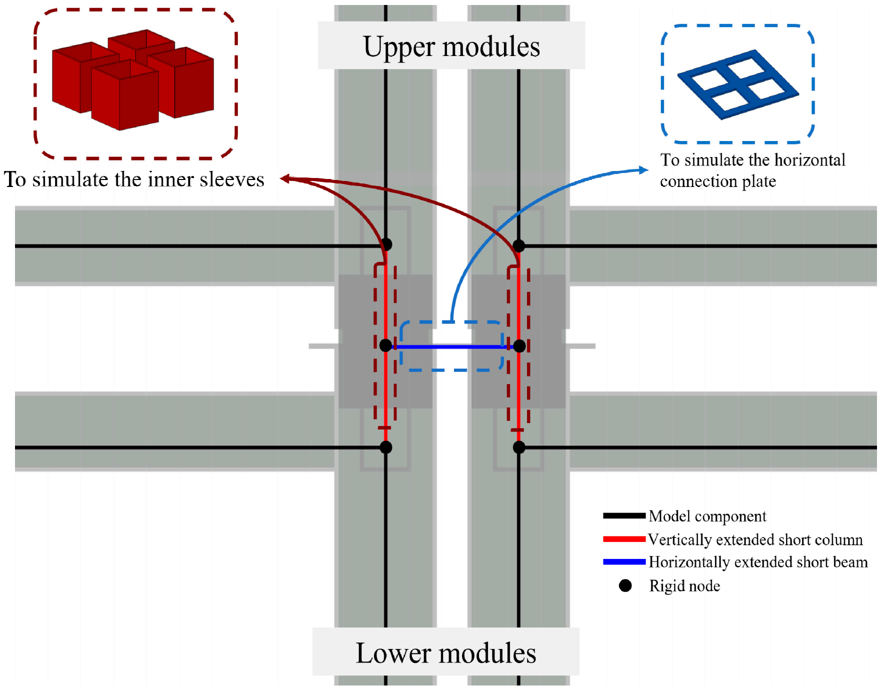

Figure 6. The connection mode of vertical modular units in MIDAS/Gen.

A spring connection is established in MIDAS/Gen, which inputs the initial stiffness values of each degree of freedom for the equivalent connection of the inter-column connectors. When the arrangement number is 1, it is positioned at the midpoint of the modular column, and when the arrangement number is 2, it is placed at the one-third and two-thirds points of the column, as shown in Figure 7.

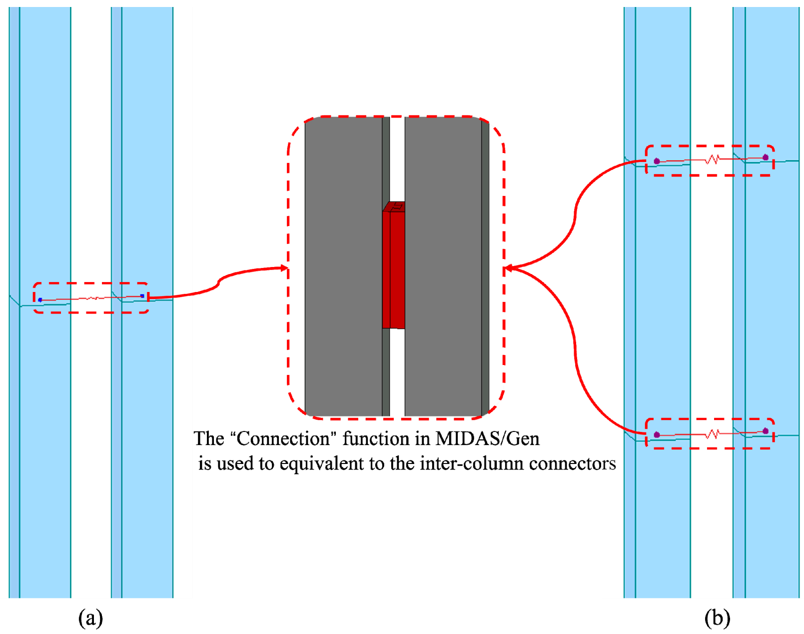

Figure 7. The connection mode of the horizontal modular unit in MIDAS/Gen: (**a**) The number of arrangements is one; (**b**) The number of arrangements is two.

Figure 8 presents the plan layout of the cooperative modular steel building. The standard floor measures 35.6 m in length and 15.2 m in width, with the five-story building totaling 15.3 m in height and each floor being 3 m high. As illustrated in Figure 9, modular units are categorized into three types based on structural form, with their dimensions and the components' section dimensions and floor parameters detailed in Table 3.

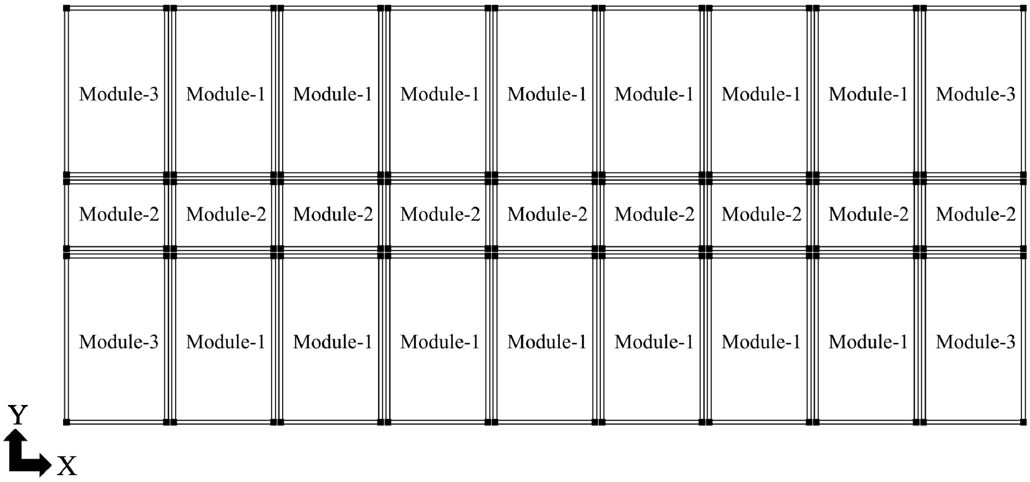

Figure 8. Cooperative modular steel building standard floor layout.

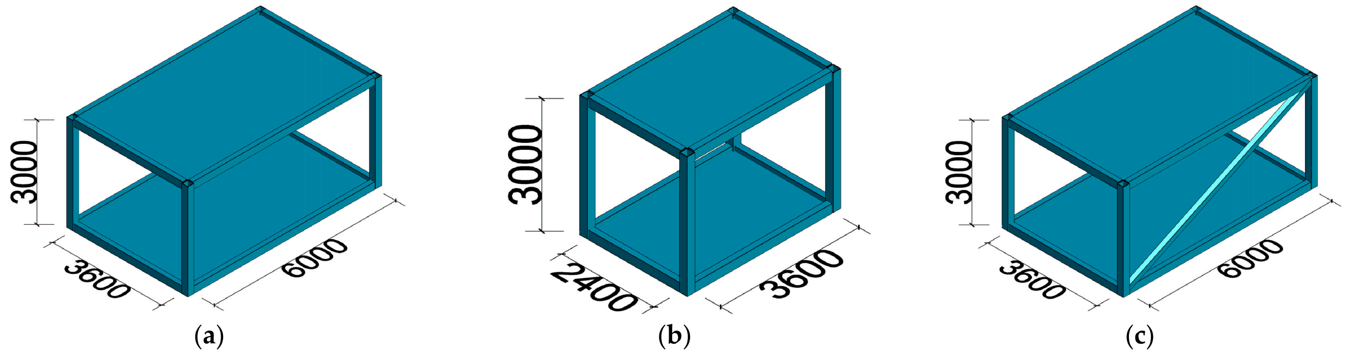

Figure 9. Types of modular units: (**a**) Module-1; (**b**) Module-2; (**c**) Module-3.

Table 3. Structural section size.

Type of Member	Section Dimensions (mm)	Materials Chosen
Modular columns	200 × 200 × 8	Q345
Floor beams	220 × 140 × 6	Q345
Ceiling beams	150 × 100 × 6	Q345
Support	140 × 140 × 4	Q235
Ceiling	20 (board thickness)	C30
Floor	120 (board thickness)	C30

4.2.2. Parameter Design

(1) Response spectrum analysis

A total of nine models are designed for response spectrum analysis to explore the displacement response of modular steel buildings under different seismic design intensities before and after cooperative force. The parameter design is shown in Table 4.

Table 4. Model parameters of response spectrum analysis.

Model Number	Seismic Fortification Intensity	Number of Inter-Column Connectors
RSA-7-0	7 degrees (0.10 g)	0
RSA-7-1	7 degrees (0.10 g)	1
RSA-7-2	7 degrees (0.10 g)	2
RSA-7.5-0	7 degrees (0.15 g)	0
RSA-7.5-1	7 degrees (0.15 g)	1
RSA-7.5-2	7 degrees (0.15 g)	2
RSA-8-0	8 degrees (0.20 g)	0
RSA-8-1	8 degrees (0.20 g)	1
RSA-8-2	8 degrees (0.20 g)	2

Note: The first number, "RSA", represents the response spectrum analysis, the second represents the seismic design intensity level, and the third represents the number of inter-column connectors.

(2) Time history analysis

Seismic wave selection

According to standard GB 50011-2010 [15], two natural waves, Elcent–h and RH2TG055, and an artificial seismic wave are selected. These waves undergo amplitude modulation and are presented in Figure 10, and their maximum seismic acceleration values under different earthquake intensities are presented in Table 5. The waves are validated against the structural base shear result and deemed suitable for dynamic time-history analysis of modular steel buildings.

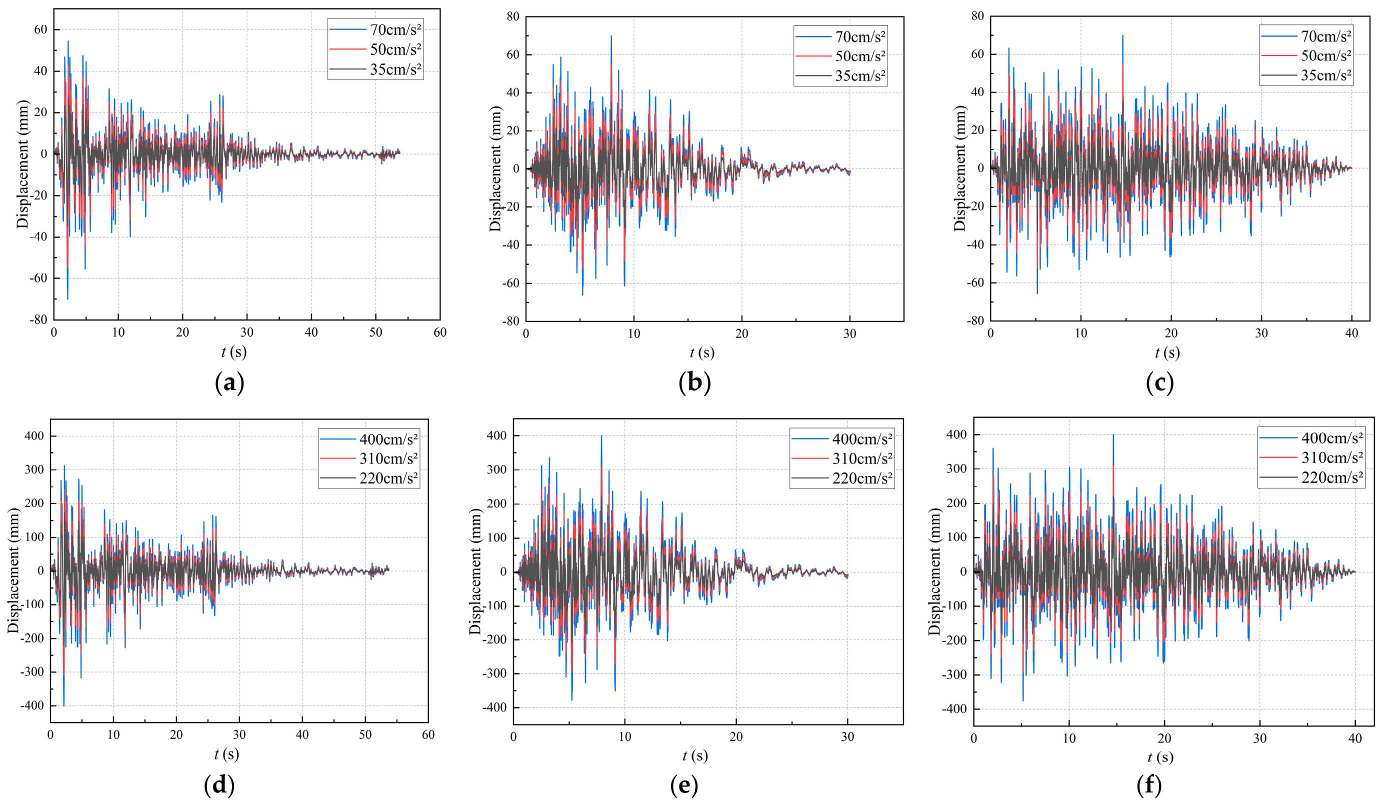

Figure 10. Time history curve of seismic wave: Frequent earthquake: (**a**) Elcent–h; (**b**) RH2TG055; (**c**) Artificial. Rare occurrence earthquake: (**d**) Elcent–h; (**e**) RH2TG055; (**f**) Artificial.

Table 5. Model parameters of time history analysis.

Model Number	Seismic Wave Number	Maximum Value of the Seismic Acceleration (cm/s^2)	Number of Inter-Column Connectors	Model Number	Seismic Wave Number	Maximum Value of the Seismic Acceleration (cm/s^2)	Number of Inter-Column Connectors
ETA-EL-35-0	EL	35	0	EPTA-EL-220-0	EL	220	0
ETA-EL-35-1	EL	35	1	EPTA-EL-220-1	EL	220	1
ETA-EL-35-2	EL	35	2	EPTA-EL-220-2	EL	220	2
ETA-RH-35-0	RH	35	0	EPTA-RH-220-0	RH	220	0
ETA-RH-35-1	RH	35	1	EPTA-RH-220-1	RH	220	1
ETA-RH-35-2	RH	35	2	EPTA-RH-220-2	RH	220	2
ETA-AW-35-0	AW	35	0	EPTA-AW-220-0	AW	220	0
ETA-AW-35-1	AW	35	1	EPTA-AW-220-1	AW	220	1
ETA-AW-35-2	AW	35	2	EPTA-AW-220-2	AW	220	2
ETA-EL-55-0	EL	55	0	EPTA-EL-310-0	EL	310	0
ETA-EL-55-1	EL	55	1	EPTA-EL-310-1	EL	310	1
ETA-EL-55-2	EL	55	2	EPTA-EL-310-2	EL	310	2
ETA-RH-55-0	RH	55	0	EPTA-RH-310-0	RH	310	0
ETA-RH-55-1	RH	55	1	EPTA-RH-310-1	RH	310	1
ETA-RH-55-2	RH	55	2	EPTA-RH-310-2	RH	310	2
ETA-AW-55-0	AW	55	0	EPTA-AW-310-0	AW	310	0
ETA-AW-55-1	AW	55	1	EPTA-AW-310-1	AW	310	1
ETA-AW-55-2	AW	55	2	EPTA-AW-310-2	AW	310	2
ETA-EL-70-0	EL	70	0	EPTA-EL-400-0	EL	400	0
ETA-EL-70-1	EL	70	1	EPTA-EL-400-1	EL	400	1
ETA-EL-70-2	EL	70	2	EPTA-EL-400-2	EL	400	2
ETA-RH-70-0	RH	70	0	EPTA-RH-400-0	RH	400	0
ETA-RH-70-1	RH	70	1	EPTA-RH-400-1	RH	400	1
ETA-RH-70-2	RH	70	2	EPTA-RH-400-2	RH	400	2
ETA-AW-70-0	AW	70	0	EPTA-AW-400-0	AW	400	0
ETA-AW-70-1	AW	70	1	EPTA-AW-400-1	AW	400	1
ETA-AW-70-2	AW	70	2	EPTA-AW-400-2	AW	400	2

Note: The first number, "ETA", denotes the elastic time history analysis, and the "EPTA" represents the elastoplastic time history analysis. The second number indicates the selected seismic wave ("EL" for Elcent–h wave, "RH" for RH2TG055 wave, and "AW" for artificial seismic wave). The third number signifies the maximum value of the seismic acceleration, while the fourth number corresponds to the number of inter-column connectors.

A total of 54 models are designed, comprising 27 for elastic time-history analysis and 27 for elastic-plastic time-history analysis. The specific parameters are shown in Table 5.

4.3. Calculation Results

4.3.1. Natural Vibration Characteristics

Figure 11 illustrates the first three vibration modes of the modular steel building. The figure reveals that the initial vibration mode of the model is X-translational, followed by the Y-translational mode, and the third mode is torsional. All models consider the first 35 orders of vibration modes. The modal mass participation ratio of all models in the first 35 orders of vibration modes in the X, Y, and Z directions reached 99.9%. Taking RSA-7-0 as an example, from the perspective of the first 10 vibration modes, the participation mass coefficient of the vibration mode in the X direction is 82.56, the Y direction is 81.99, and the Z direction is 81.96. The participation mass coefficient of the vibration mode in the X translation is the largest. Other models show similar laws. Table 6 compares the natural vibration periods of different models. The natural vibration period characteristics of all models demonstrate a consistent trend: as the number of connectors increases, the fundamental period of the structure diminishes. This decrease suggests that introducing inter-column connectors enhances structural stiffness and reduces the fundamental period.

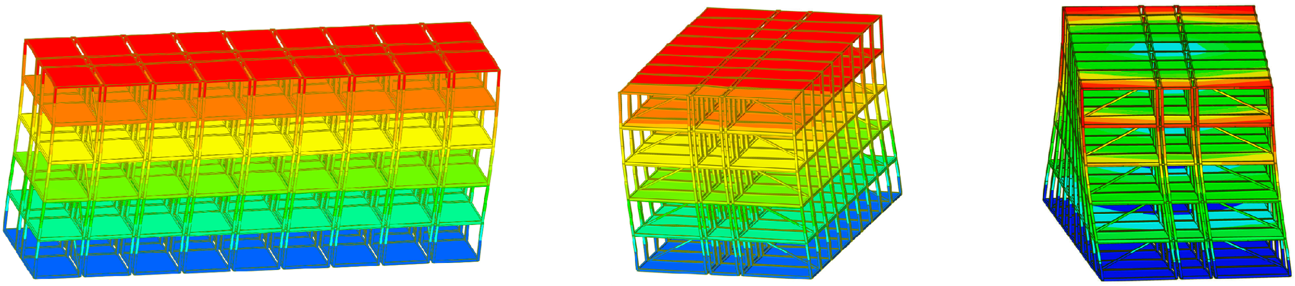

(**a**) (**b**) (**c**)

Figure 11. Comparison of the first three modes of the structure: (**a**) The first vibration mode: translation in the X-direction; (**b**) The second vibration mode: translation in the X-direction; (**c**) The third vibration mode: torsion.

Table 6. Structural natural vibration period of different models.

Seismic Fortification Intensity	Model Number	Natural Vibration Period (s)
7 degrees (0.10 g)	RSA-7-0	0.830
	RSA-7-1	0.659
	RSA-7-2	0.636
7 degrees (0.15 g)	RSA-7.5-0	0.830
	RSA-7.5-1	0.659
	RSA-7.5-2	0.636
8 degrees (0.20 g)	RSA-8-0	0.830
	RSA-8-1	0.659
	RSA-8-2	0.636

4.3.2. Response Spectrum Analysis

Table 7 presents the peak displacement of each numerical model in the X and Y directions under frequent earthquakes, with the inter-story displacement angle depicted in Figure 12. Under three design intensities, the maximum inter-story displacement angle of the building occurs in the second story. With a seismic fortification intensity of 8 degrees (0.20 g) and an increase in number of connectors from zero to one, the top displacement decreases from 28.32 mm to 23.72 mm, a reduction of 16.2%, and the maximum decrease in inter-story displacement angle is 36.1%. Increasing the number of connectors from one to two results in a maximum top displacement reduction of 2.1% and a maximum inter-story displacement angle reduction of 13.1%. The inter-story displacement angles on the fourth and fifth floors of the cooperative modular steel building are larger than those in the non-cooperative modular building. This is because the cooperative force between the modular components increases the overall structural stiffness, resulting in increased base shear and significantly higher shear force at the top floor, thereby elevating the inter-story displacement.

The T/CECS 507-2018 *Technical specification for steel modular buildings* [18] stipulates that the inter-story displacement angle of the modular building under frequent earthquake loads should be less than height/300, and the elastic-plastic inter-story displacement angle of the modular building under rare earthquakes should be less than height/50. The inter-story displacement angles of all numerical models remain within the limit (≤story height/300) specified in T/CECS 507-2018. The lateral stiffness of the building in the Y-direction is significantly enhanced due to the transverse support in the modular building, resulting in smaller top displacement and inter-story displacement angles in the Y-direction compared to the X-direction. When the design seismic fortification intensity is 7 degrees (0.10 g) and 7 degrees (0.15 g), the building's displacement response exhibits a similar pattern to that at 8 degrees (0.20 g). The findings indicate that increasing the number of inter-column connectors from zero to one for modular steel buildings significantly improves lateral performance. However, after achieving cooperative force in the modular components, the impact of adding more inter-column connectors on enhancing lateral performance becomes relatively less pronounced.

Table 7. Top displacement of modular steel buildings with different seismic fortification intensities.

Seismic Fortification Intensity	Model Number	Top Displacement (mm)	
		X-Direction	Y-Direction
7 degrees (0.10 g)	RSA-7-0	14.16	10.77
	RSA-7-1	11.86	9.90
	RSA-7-2	11.62	9.65
7 degrees (0.15 g)	RSA-7.5-0	21.24	16.15
	RSA-7.5-1	17.79	14.85
	RSA-7.5-2	17.43	14.47
8 degrees (0.20 g)	RSA-8-0	28.32	21.53
	RSA-8-1	23.72	19.80
	RSA-8-2	23.24	19.29

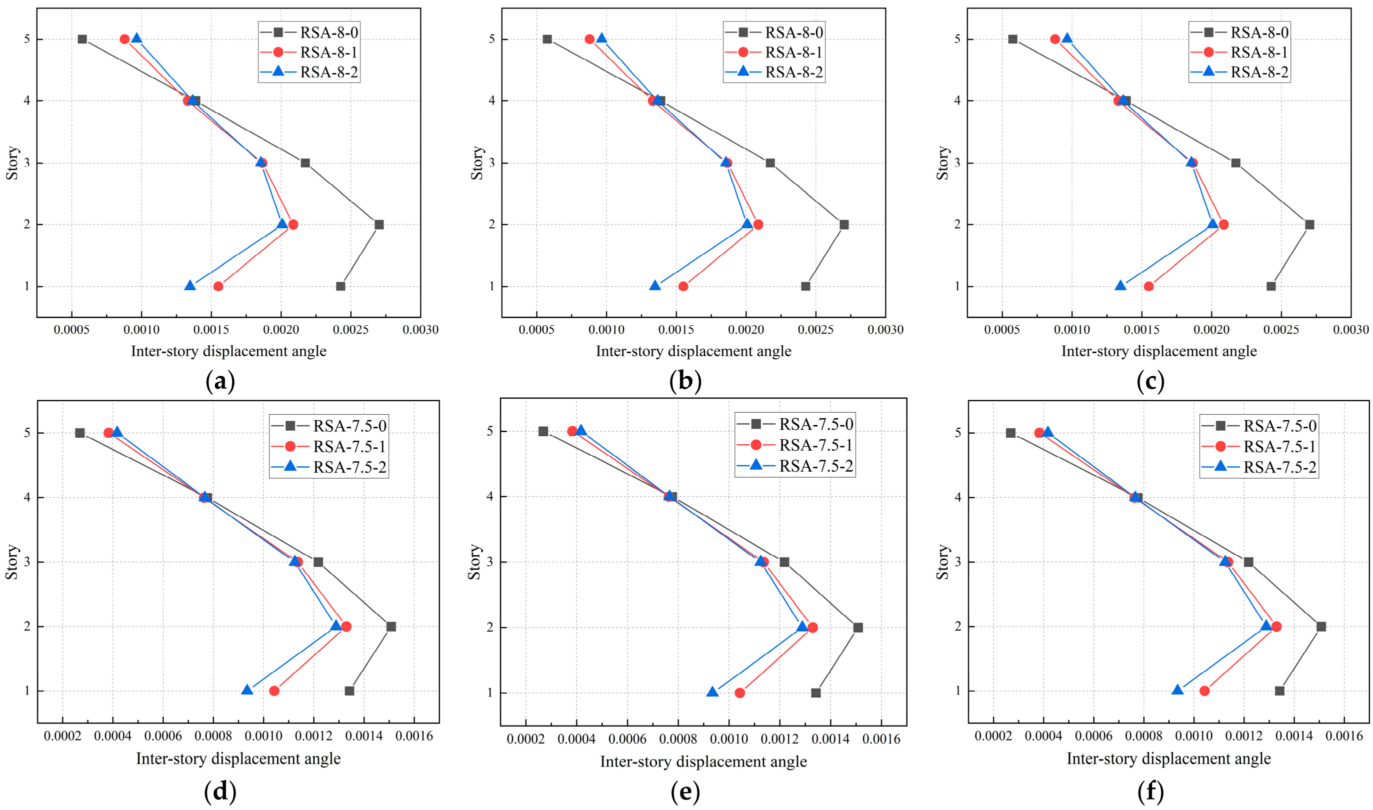

Figure 12. Inter-story displacement angle of a modular steel building with different seismic fortification intensities: (**a**) 7-degree (0.10 g) in the X-direction; (**b**) 7-degree (0.15 g) in the X-direction; (**c**) 8-degree (0.20 g) in the X-direction; (**d**) 7-degree (0.10 g) in the Y-direction; (**e**) 7-degree (0.15 g) in the Y-direction; (**f**) 8-degree (0.20 g) in the Y-direction.

4.3.3. Elastic Time History Analysis

The inter-story displacement of 27 numerical models under various earthquake peak accelerations is depicted in Figures 13–15. The maximum inter-story displacement angle for all numerical models occurs on the second floor. In the cooperative modular steel building, the inter-story displacement angle at the bottom story is substantially reduced compared to that in the non-cooperative modular steel building. This reduction is attributed to the building's lateral support, which increases the lateral stiffness in the Y-direction, consequently diminishing the inter-story displacement angle in this direction compared to the X-direction. The displacement response of the numerical models using elastic time-history analysis parallels the results from the response spectrum analysis.

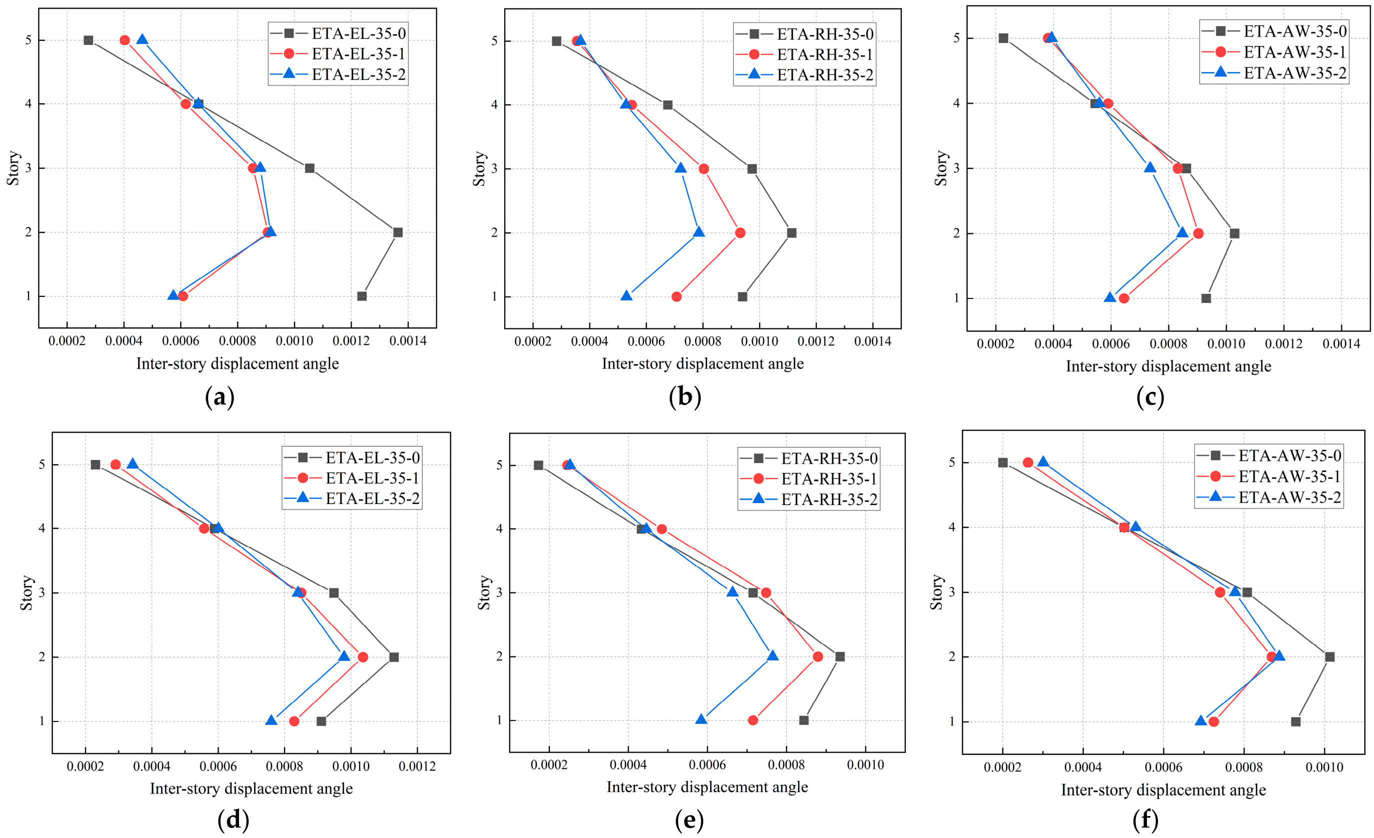

Figure 13. The inter-story displacement angle of the modular steel building when the peak acceleration of the earthquake is 35 cm/s^2: (**a**) Elcent–h wave in the X-direction; (**b**) RH2TG055 wave in the X-direction; (**c**) Artificial wave in the X-direction; (**d**) Elcent–h wave in the Y-direction; (**e**) RH2TG055 wave in the Y-direction; (**f**) Artificial wave in the Y-direction.

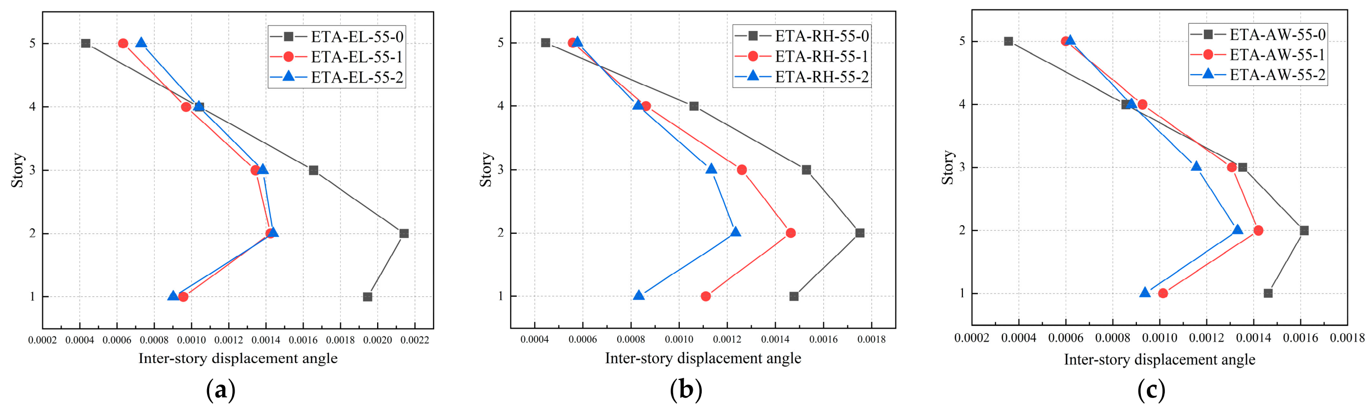

Figure 14. *Cont.*

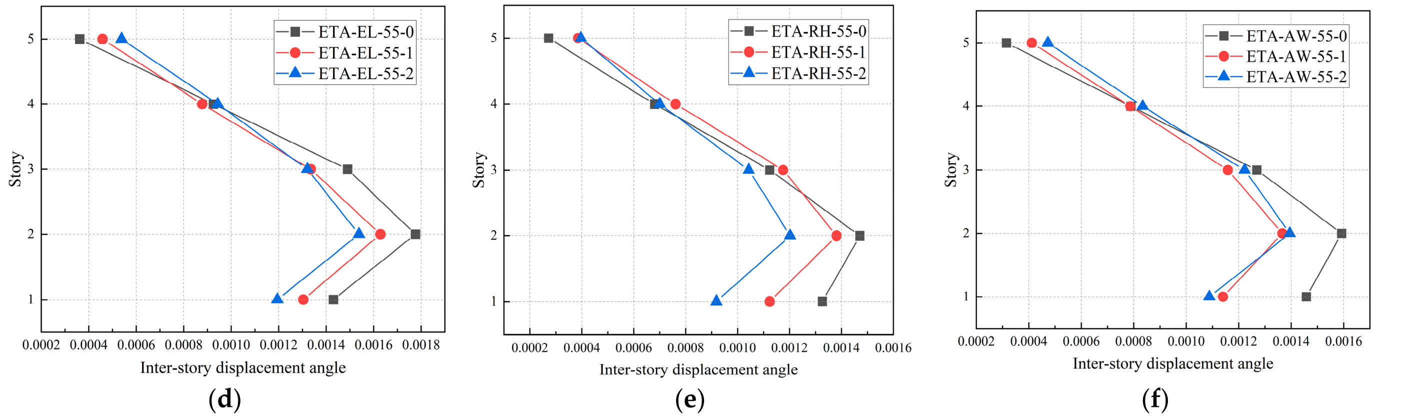

Figure 14. The inter-story displacement angle of the modular steel building when the peak acceleration of the earthquake is 55 cm/s^2: (**a**) Elcent–h wave in the X-direction; (**b**) RH2TG055 wave in the X-direction; (**c**) Artificial wave in the X-direction; (**d**) Elcent–h wave in the Y-direction; (**e**) RH2TG055 wave in the Y-direction; (**f**) Artificial wave in the Y-direction.

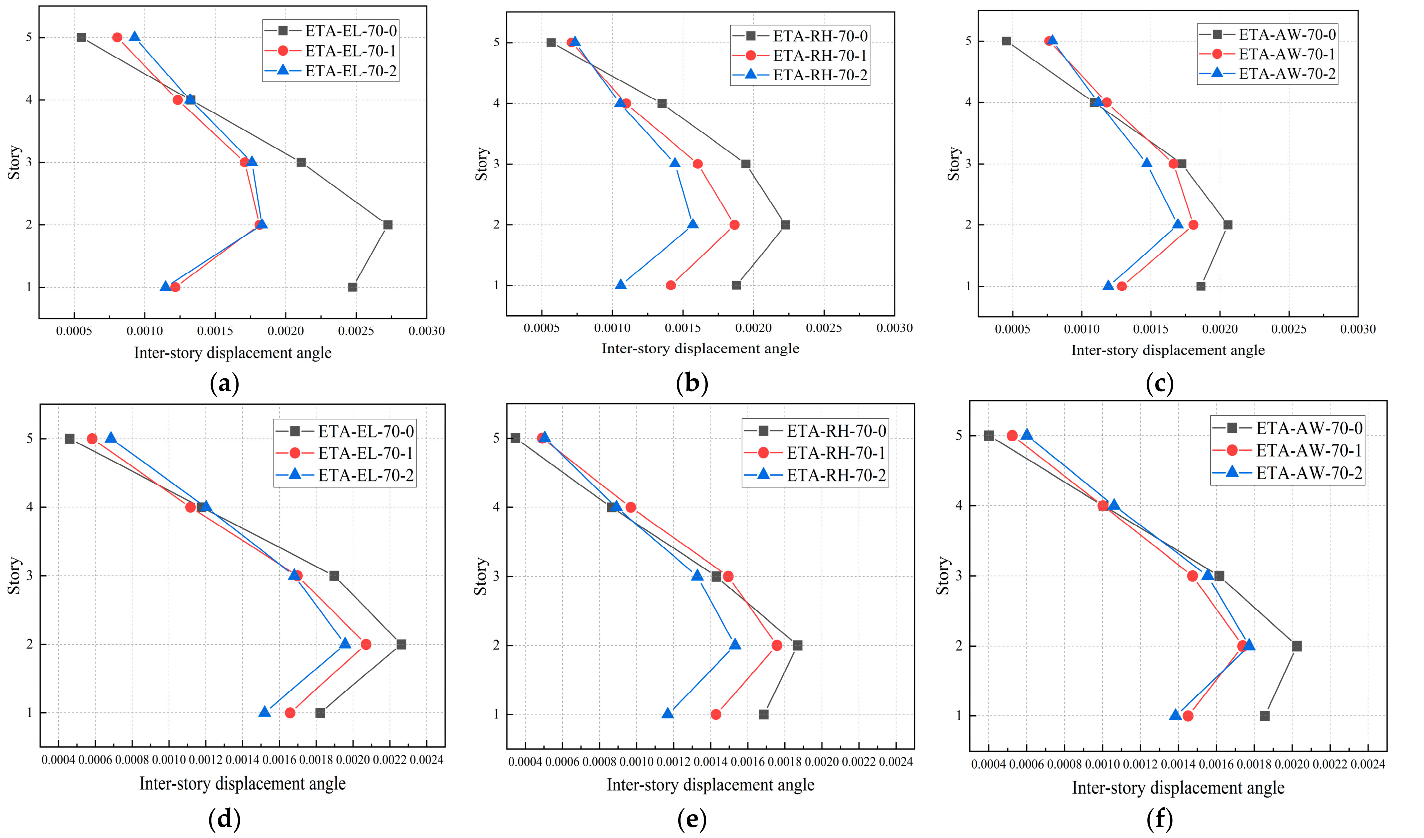

Figure 15. The inter-story displacement angle of the modular steel building when the peak acceleration of the earthquake is 70 cm/s^2: (**a**) Elcent–h wave in the X-direction; (**b**) RH2TG055 wave in the X-direction; (**c**) Artificial wave in the X-direction; (**d**) Elcent–h wave in the Y-direction; (**e**) RH2TG055 wave in the Y-direction; (**f**) Artificial wave in the Y-direction.

4.3.4. Elastoplastic Time History Analysis

The elastic-plastic time-history analysis of modular steel buildings focuses on the top displacement, inter-story displacement angle, and base shear in the X-direction. This analysis compares the variation in the structural response of the modular steel building under rare earthquakes, both before and after the application of cooperative forces.

(1) Top displacement time histories

Displacement time histories in the X-direction at the top, as illustrated in Figures 16–18, are compared under different seismic peak accelerations. It is evident from the diagrams that achieving cooperative force in the modular steel building markedly reduces the maximum top displacement.

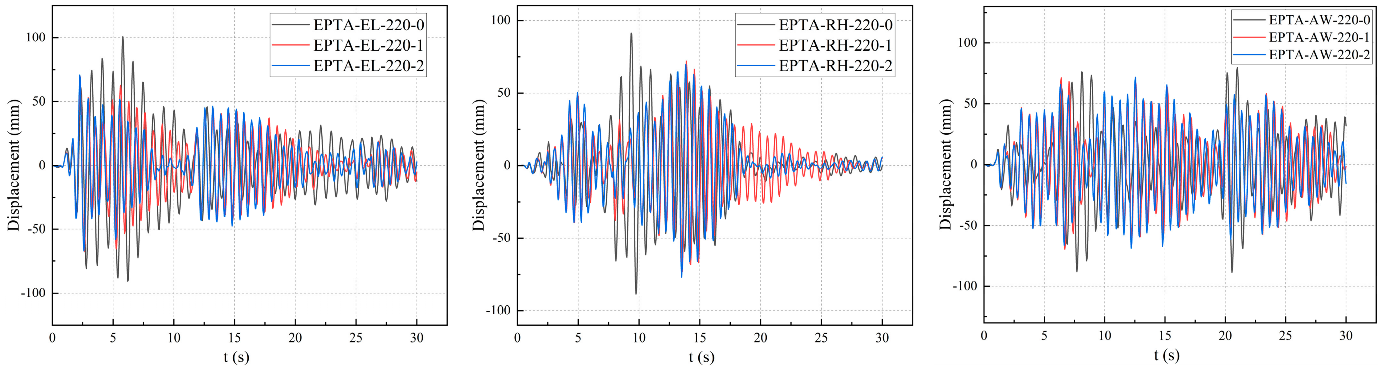

(**a**) (**b**) (**c**)

Figure 16. The top displacement of the modular steel building when the seismic peak acceleration is 220 cm/s^2: (**a**) Elcent–h; (**b**) RH2TG055; (**c**) Artificial.

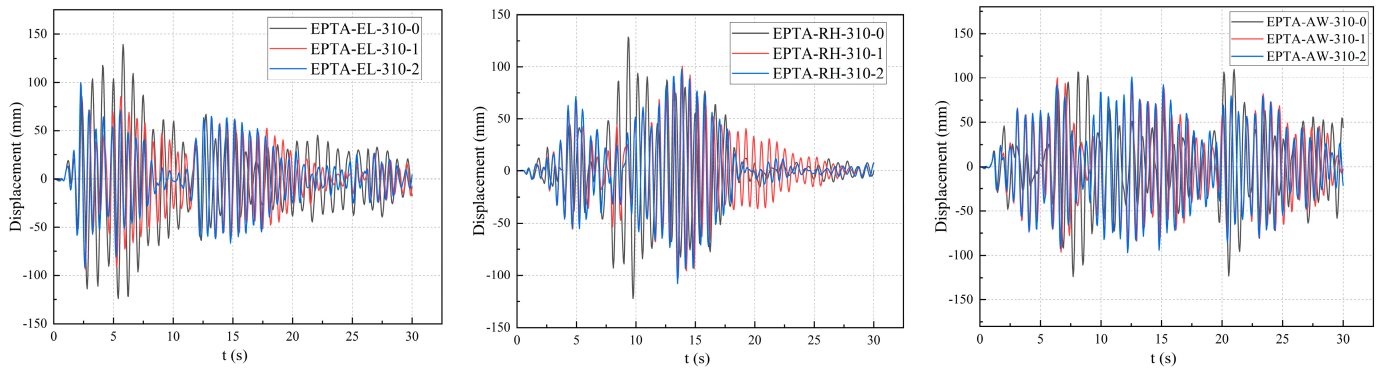

(**a**) (**b**) (**c**)

Figure 17. The top displacement of the modular steel building when the seismic peak acceleration is 310 cm/s^2: (**a**) Elcent–h; (**b**) RH2TG055; (**c**) Artificial.

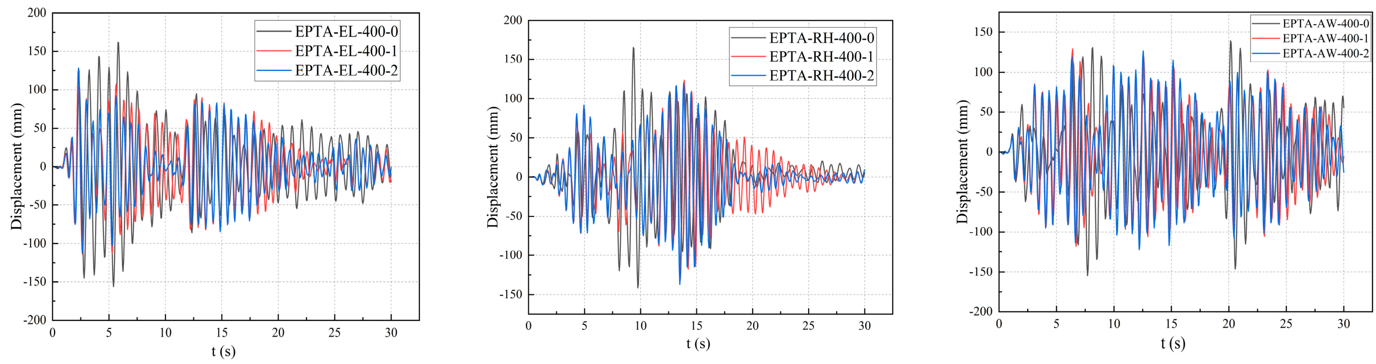

(**a**) (**b**) (**c**)

Figure 18. The top displacement of the modular steel building when the seismic peak acceleration is 400 cm/s^2: (**a**) Elcent–h; (**b**) RH2TG055; (**c**) Artificial.

(2) inter-story displacement angle

Figures 19–21 display the inter-story displacement angle of the model under diverse seismic waves. When subjected to seismic waves with varying seismic peak accelerations, the structural model remains within the 1/50 limit for the inter-story displacement angle as specified in the standard [18]. In contrast to its non-cooperative counterpart, the cooperative modular steel building exhibits reduced inter-story displacement in the weak story, thereby enhancing the building's safety in rare earthquakes and more easily conforming to the standard requirements.

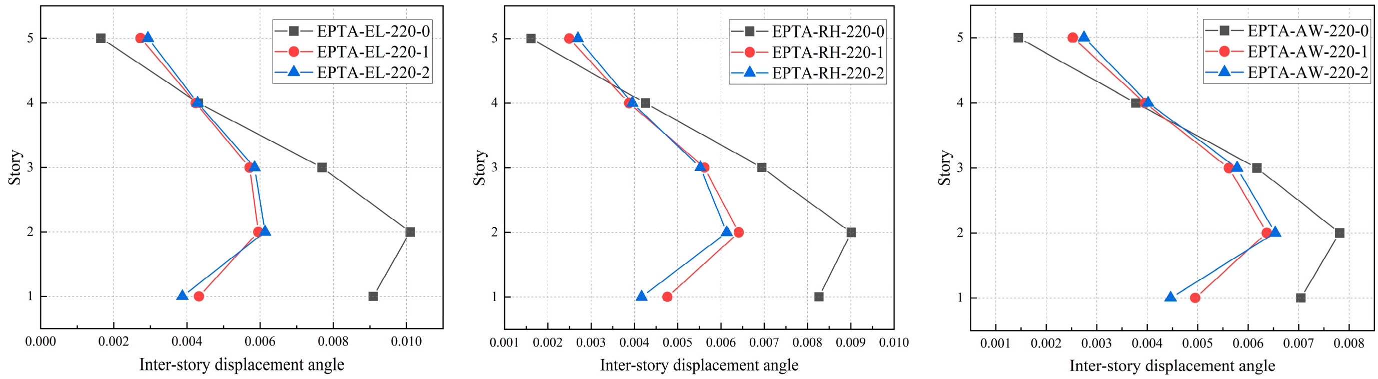

(**a**) (**b**) (**c**)

Figure 19. The inter-story displacement angle of the modular steel building when the peak acceleration of the earthquake is 220 cm/s^2: (**a**) Elcent–h; (**b**) RH2TG055; (**c**) Artificial.

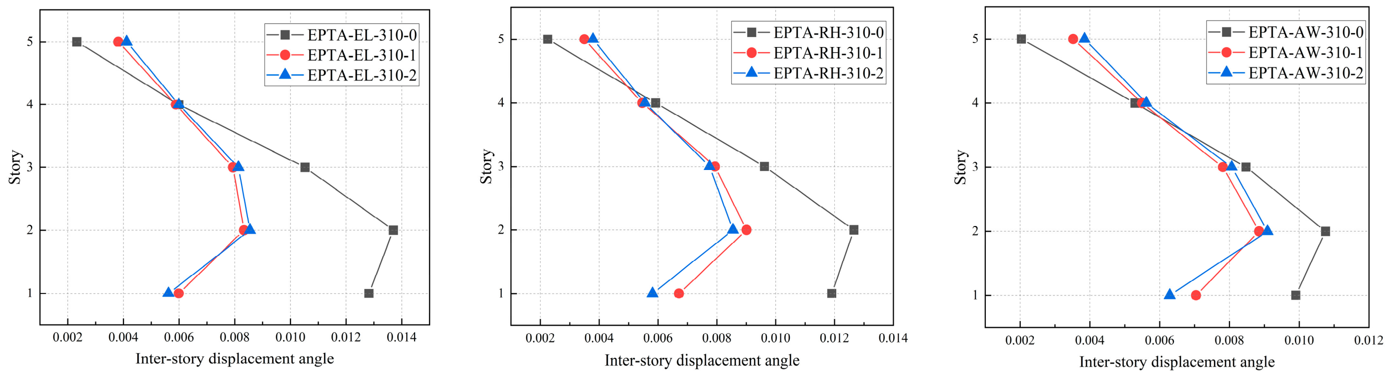

(**a**) (**b**) (**c**)

Figure 20. The inter-story displacement angle of the modular steel building when the peak acceleration of the earthquake is 310 cm/s^2: (**a**) Elcent–h; (**b**) RH2TG055; (**c**) Artificial.

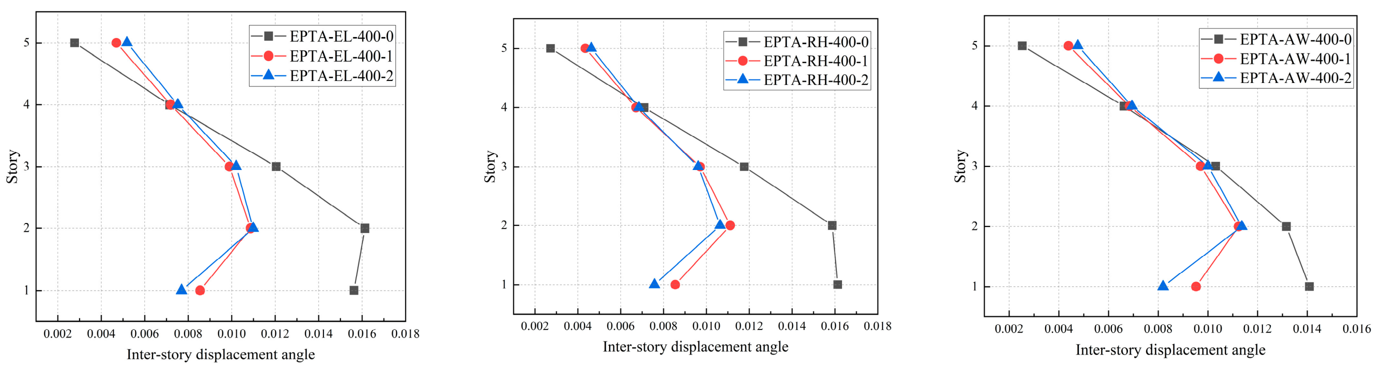

(**a**) (**b**) (**c**)

Figure 21. The inter-story displacement angle of the modular steel building when the peak acceleration of the earthquake is 400 cm/s^2: (**a**) Elcent–h; (**b**) RH2TG055; (**c**) Artificial.

(3) Base shear

The base shear time histories for each numerical model under different rare seismic waves are shown in Figures 22–24. Under the influence of seismic waves with varied seismic peak accelerations, the cooperative modular steel building demonstrates an increased base shear trend compared to the non-cooperative building. This increase can be attributed to improved structural stiffness, a result of the collaborative efforts of modular unit columns, which reduces the natural vibration period. As the period decreases, the seismic influence coefficient escalates, amplifying the earthquake-induced base shear force.

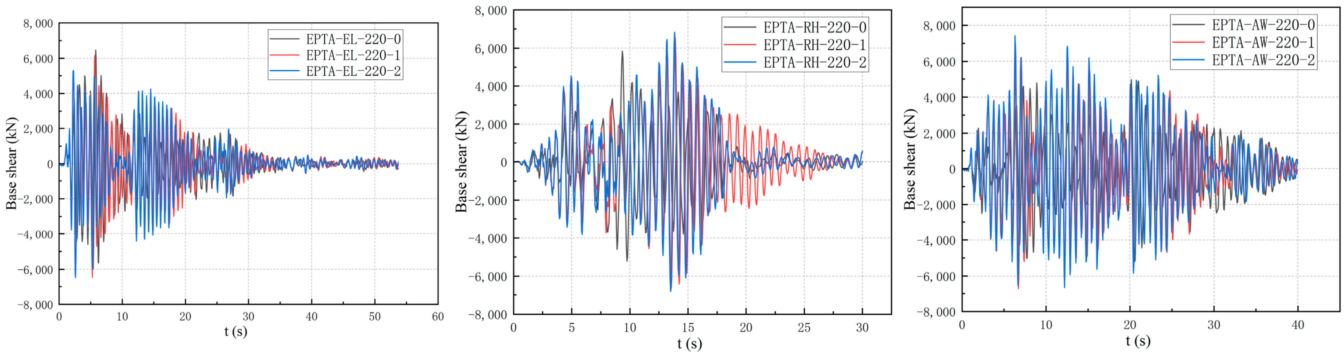

(**a**) (**b**) (**c**)

Figure 22. The base shear of the modular steel building when the peak acceleration of the earthquake is 220 cm/s^2: (**a**) Elcent–h; (**b**) RH2TG055; (**c**) Artificial.

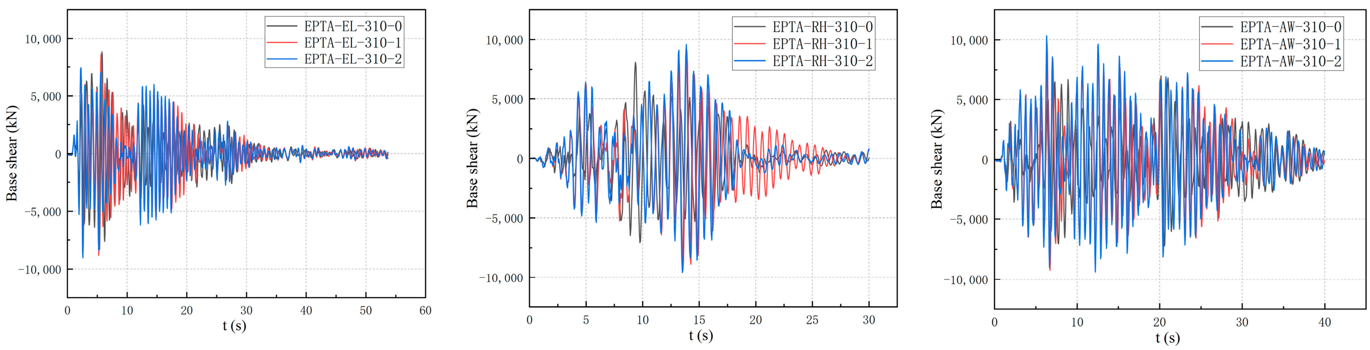

(**a**) (**b**) (**c**)

Figure 23. The base shear of the modular steel building when the peak acceleration of the earthquake is 310 cm/s^2: (**a**) Elcent–h; (**b**) RH2TG055; (**c**) Artificial.

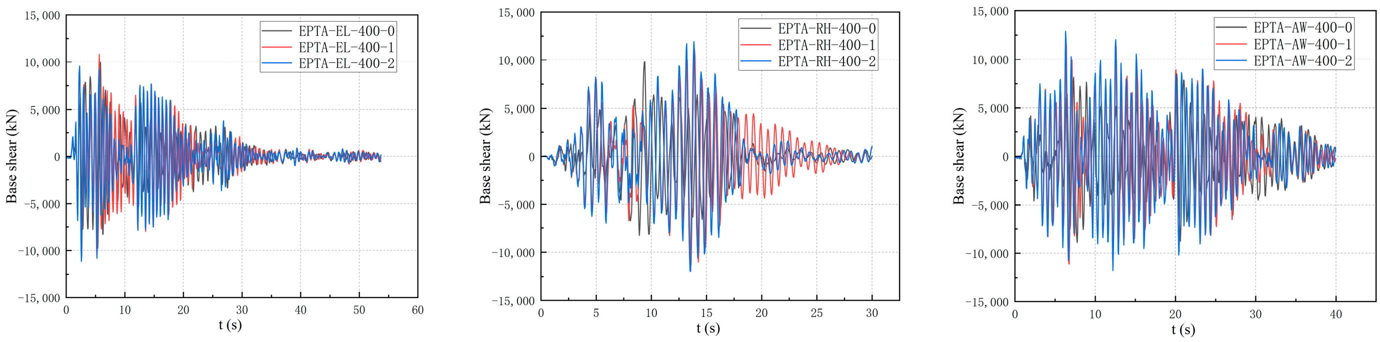

(**a**) (**b**) (**c**)

Figure 24. The base shear of the modular steel building when the peak acceleration of the earthquake is 400 cm/s^2: (**a**) Elcent–h; (**b**) RH2TG055; (**c**) Artificial.

5. Applicable Height

5.1. Modeling Scheme

According to the T/CECS 507-2018 *technical specification for steel structure modular buildings* [18], *GB 50011-2010* Code for Seismic Design of Buildings [15], and *GB 50009-2012* Load Code for the design of building structures [16], this section mandates that the elastic inter-story displacement angle of 1/300 under frequent earthquakes is the limit value, and the maximum stress ratio of components should be less than 0.85. This study explores the variation in the modular steel building system's calculation results under synergistic force, considering changes in seismic fortification intensity and building height. The seismic fortification intensity is examined in three scenarios: 7 degrees (0.10 g), 7 degrees (0.15 g), and 8 degrees (0.20 g). The module type and layout are depicted in Figure 25. The seismic period reduction factor is set at 0.7. The modular unit size, component section size, and floor parameters used are consistent with those in Chapter 4.

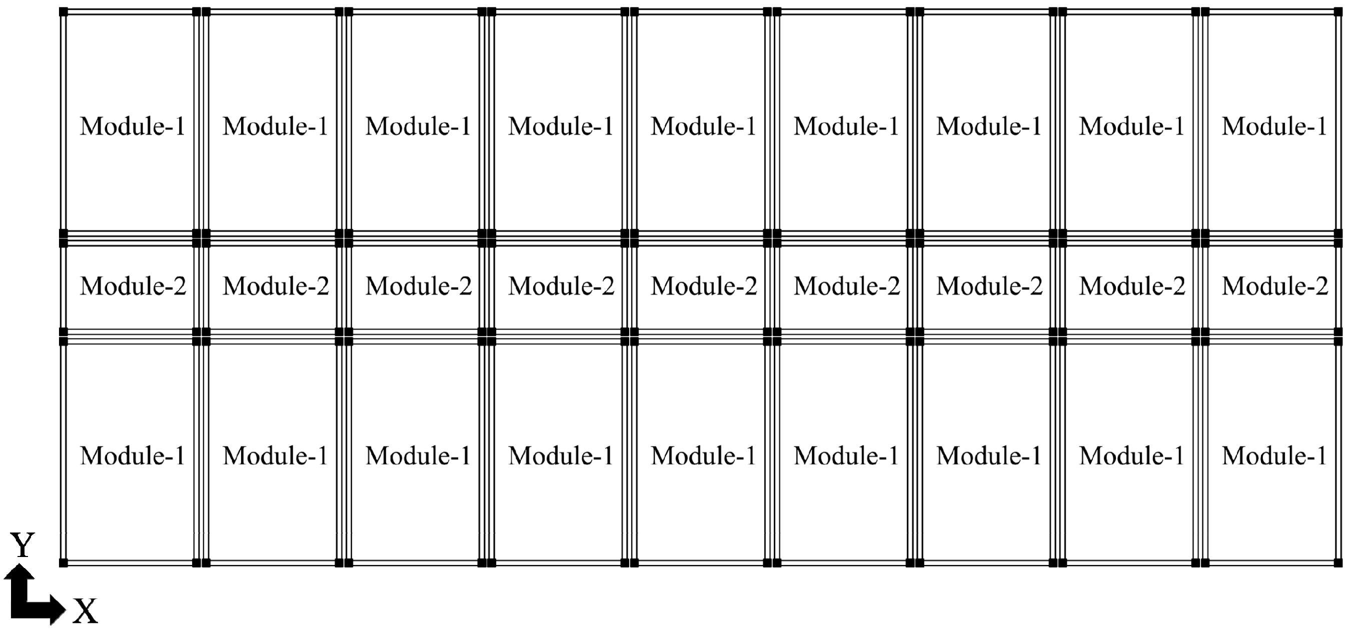

Figure 25. Modular steel building standard-story module layout.

5.2. Parameter Design

In this section, a total of six models are designed to explore the applicable height range of cooperative modular steel buildings in different seismic fortification intensity areas. The numerical model parameters are detailed in Table 8.

Table 8. Model parameters suitable for height analysis.

Model Number	Seismic Fortification Intensity	Number of Inter-Column Connectors
HA-7-1	7 degrees (0.10 g)	1
HA-7.5-1	7 degrees (0.15 g)	1
HA-8-1	8 degrees (0.20 g)	1
HA-7-2	7 degrees (0.10 g)	2
HA-7.5-2	7 degrees (0.15 g)	2
HA-8-2	8 degrees (0.20 g)	2

Note: The first number, "HA", represents the height analysis, the second number represents the seismic design intensity, and the third number represents the number of inter-column connectors.

5.3. Applicable Height

Figures 26 and 27 reveal that the inter-story displacement angle of model HA-7-1 does not exceed the 1/300 limit when its height is eight stories. However, the maximum stress ratio of the component surpasses the 0.85 threshold. Similarly, for model HA-7.5-1 (an eight-story building), its inter-story displacement angle remains within acceptable limits, but its maximum stress ratio exceeds the predefined value. When the HA-8-1 model (a six-story building) is analyzed, its inter-story displacement angle exceeds the allowable value, while at the height of five stories, its maximum stress ratio does not meet the established requirements.

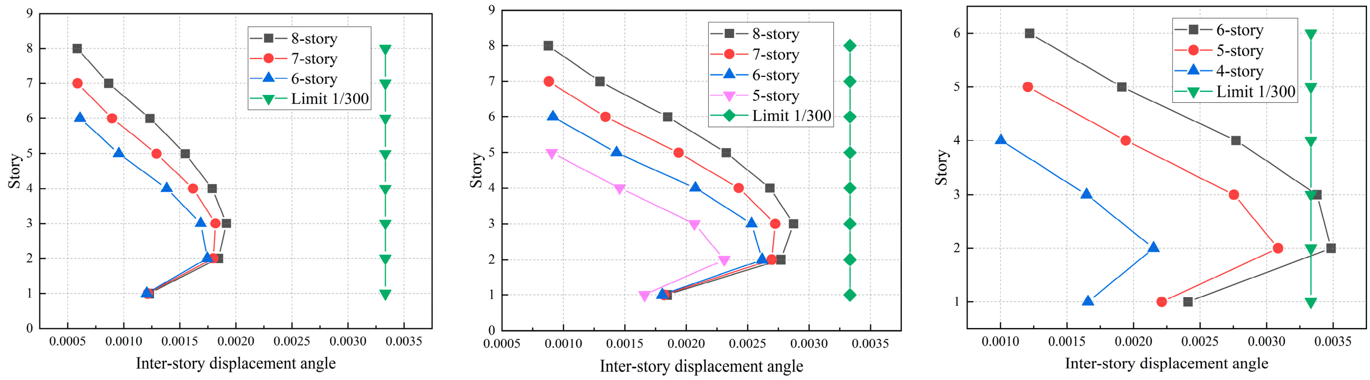

(**a**) (**b**) (**c**)

Figure 26. Variation of interlayer displacement angle when the number of connectors is one: (**a**) HA-7-1; (**b**) HA-7.5-1; (**c**) HA-8-1.

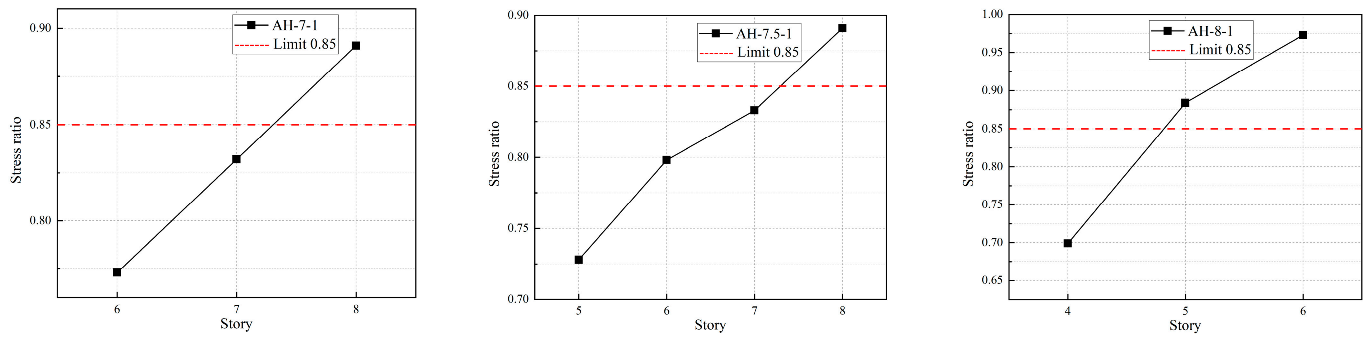

(**a**) (**b**) (**c**)

Figure 27. Variation of the maximum stress ratio when the number of connectors is one: (**a**) HA-7-1; (**b**) HA-7.5-1; (**c**) HA-8-1.

Figures 28 and 29 indicate that for HA-7-2 with eight stories, the component's maximum stress ratio surpasses the limit. This trend is also evident in HA-7.5-2, with eight stories, where the maximum stress ratio exceeds the set threshold. Moreover, when HA-8-2 comprises only six stories, both the maximum stress ratio and the inter-story displacement angle of the component exceed their respective limits. Additionally, with a five-story configuration, the component exhibits a maximum stress ratio of 0.852, failing to comply with the specified limits. The analysis suggests that in fortification intensities ranging from level 7 to level 8, controlling the story count in cooperative modular steel buildings primarily depends on managing the component's maximum stress ratio. Under identical seismic fortification intensity and story count conditions, increasing the number of connectors can effectively reduce the maximum stress ratio.

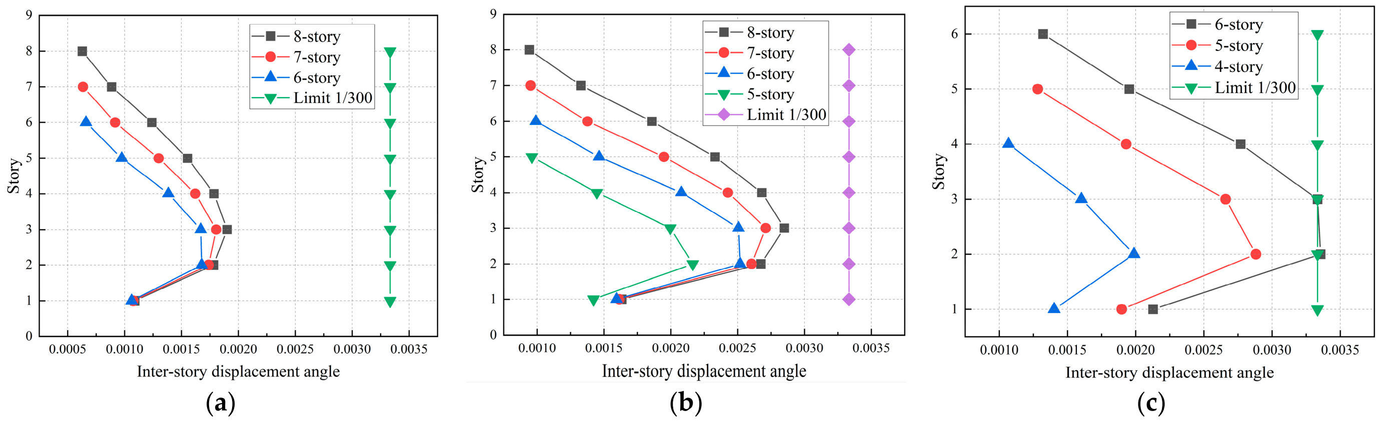

Figure 28. Variation of interlayer displacement angle when the number of connectors is two: (**a**) HA-7-1; (**b**) HA-7.5-1; (**c**) HA-8-1.

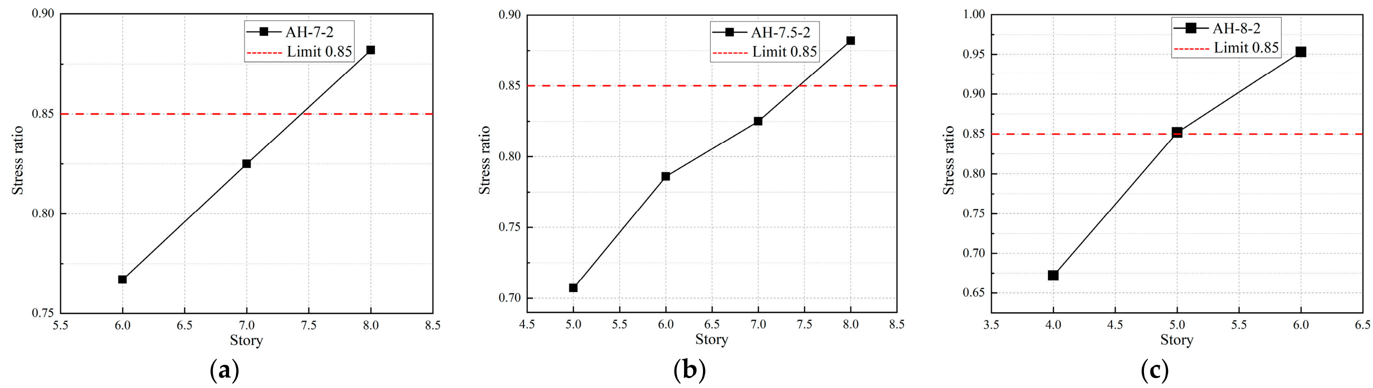

Figure 29. Variation of the maximum stress ratio when the number of connectors is two: (**a**) HA-7-1; (**b**) HA-7.5-1; (**c**) HA-8-1.

The scope of application for the modular steel building system under each seismic fortification intensity is detailed in Table 9, and the maximum applicable height of the modular steel building stipulated in the T/CECS 507-2018 *technical specification for steel structure modular buildings* [18] is detailed in Table 10. The comparison shows that under the same seismic fortification intensity, the cooperative modular steel building has a higher building height.

Table 9. The maximum applicable height of the cooperative modular steel building system.

Number of Inter-Column Connectors	Seismic Fortification Intensity	Number of Stories	Applicable Height (m)
1	7 degrees (0.10 g)	7	21
	7 degrees (0.15 g)	7	21
	8 degrees (0.20 g)	4	12
2	7 degrees (0.10 g)	7	21
	7 degrees (0.15 g)	7	21
	8 degrees (0.20 g)	4	12

Table 10. The maximum applicable height of the modular steel building stipulated in the T/CECS 507-2018 *technical specification for steel structure modular buildings* [18].

Seismic Fortification Intensity	Number of Stories	Applicable Height (m)
7 degrees (0.10 g)	3	9
7 degrees (0.15 g)	3	9
8 degrees (0.20 g)	1~2	3~6

6. Conclusions

This study numerically investigates the lateral performance and applicable height of modular steel buildings with inter-column connectors. Within the study context, the influence of the number of connectors and type of seismic action on the lateral performance and applicable height of the structure is analyzed. The following conclusions are drawn:

(1) The finite element simulation is conducted to analyze the inter-column connector, and the initial stiffness of the six degrees of freedom of the connector is calculated. The results indicate that the inter-column connectors can effectively transmit the internal force generated by the work between modular unit columns.

(2) Design a five-story modular steel building and carry out finite element modeling. Compare and analyze the cooperative modular steel building and the non-cooperative modular steel building, and perform response spectrum analysis, elastic time history analysis, and elastic-plastic time history analysis. After sorting out and analyzing, the following main conclusions are drawn:

1. The calculation results show that the inter-story displacement angle at the bottom of the cooperative modular steel building and the displacement of the top story of the building are smaller than those of the non-cooperative modular steel building. The maximum reduction of the inter-story displacement angle can reach 36.1%, and the maximum reduction of the top displacement can reach 16.2%, indicating that the modular building of the cooperative force has better lateral performance.

2. Under the same seismic action, compared with the non-cooperative modular steel building, the base shear of the cooperative modular steel building is larger, indicating that the overall stiffness of the structure has increased.

3. Compared with the non-cooperative modular steel building, the cooperative steel building has better displacement response and greater structural safety redundancy under rare earthquakes, which provides a new idea and scheme for the promotion of modular steel buildings in earthquake-prone areas.

(3) The finite element analysis of the cooperative modular steel building is carried out. Considering the change in seismic fortification intensity and the number of stories, the displacement response and internal force change of the cooperative modular steel building system are observed. After analysis and comparison, the applicable height range of the system is obtained. The results show that, compared with the non-cooperative modular steel building in the same seismic intensity area, the number of building layers in the cooperatively stressed modular steel structure is higher. It is recommended that the cooperative modular steel building height be 21 m when the seismic fortification intensity is 7 degrees (0.10 g), 7 degrees (0.15 g) is 21 m, and 8 degrees (0.20 g) is 12 m.

The research results provide important implications for design practice and future research on modular steel buildings. Specifically, based on the newly proposed inter-column connector, this paper studies the improvement of the lateral resistance and applicable height of the cooperative steel modular building compared with the non-cooperative modular steel building, which provides a new method for the popularization and application of the modular building in high-intensity areas. At the same time, the inter-column connector also provides valuable references for the connection design of other modular buildings.

However, since the results of this study were obtained in the context of a five-story steel modular building with a typical plan, changing the type of module unit, building height, plane layout, and building geometry may affect some structural response analysis results.

These changes can be resolved in future research. In addition, under the action of horizontal seismic force, the relative shear displacement between adjacent modular columns is small. Therefore, the elastic stage of the inter-column connector is considered conservatively in this paper. In future research, the contribution of the plastic stage of the connectors to the lateral resistance of the whole structure should also be considered. In addition, the influence of foundation vibration isolation technology on the seismic performance of modular buildings can also be considered [19,20]. The finite-element analysis method can be further improved and structurally analyzed by using meshless approaches that are more generalized than the finite-element method [21,22]. Furthermore, we investigated the free lateral and transverse vibrations of bidirectionally modular beams interconnected by lateral and transverse springs in the framework of the nonlocal elasticity theory. The theory mentioned above is more general than that of classical elasticity theory, which is commonly utilized for structural analyses of macrosystems [23,24].

Author Contributions: Conceptualization, methodology, and funding acquisition, Y.W. and Q.A.; project administration, Y.W. and Q.A.; analysis, Q.A. and Z.H.; writing—original draft, Z.H.; writing—review and editing, Q.A.; All authors have read and agreed to the published version of the manuscript.

Funding: The project received financial support from the National Natural Science Foundation of China (grant numbers 52208175 and 52078258). All statements, results, and conclusions are those of the researchers and do not necessarily reflect the views of these foundations.

Data Availability Statement: The data presented in this study are available on request from the authors. The data are not publicly available due to privacy.

Acknowledgments: The authors also sincerely thank the anonymous reviewers for their insightful comments and suggestions.

Conflicts of Interest: The authors declare that they have no known competing financial interests or personal relationships that could have appeared to influence the work reported in this paper.

References

1. Sha, X.; Liu, X.; Wang, Y.; Zeng, M. The development status and trend of modular steel structure system. *Ind. Build.* **2023**, 1–19. Available online: https://kns.cnki.net/kcms/detail/11.2068.TU.20230314.1308.003.html (accessed on 6 November 2023). (In Chinese)
2. Tian, X.; Liu, X.; Liu, Y.; Chen, Y.; Liu, Y. Research progress of connection joints between modules of column-bearing modular steel structure buildings. *Dev. Build. Steel Struct.* **2022**, *24*, 197–205. (In Chinese)
3. Yang, C.; Xu, B.; Xia, J.; Chang, H.; Chen, X.; Ma, R. Mechanical Behaviors of Inter-Module Connections and Assembled Joints in Modular Steel Buildings: A Comprehensive Review. *Buildings* **2023**, *13*, 1727. [CrossRef]
4. Lawson, M.; Ogden, R.; Goodier, C. *Design in Modular Construction*; CRC Press: Boca Raton, FL, USA, 2014; ISBN 0-415-55450-0.
5. Liu, M.Y.; Wang, Y.; Jia, S.S. Study on mechanical properties of new modular steel frame plate inner sleeve connection joint. *Steel Struct.* **2018**, *33*, 1–5+10. (In Chinese)
6. Chen, Z.; Wang, J.; Liu, J.; Khan, K. Seismic Behavior and Moment Transfer Capacity of an Innovative Self-Locking Inter-Module Connection for Modular Steel Building. *Eng. Struct.* **2021**, *245*, 112978. [CrossRef]
7. Palazzo, B.; Castaldo, P.; Marino, I. The Dissipative Column: A New Hysteretic Damper. *Buildings* **2015**, *5*, 163–178. [CrossRef]
8. Sharafi, P.; Mortazavi, M.; Samali, B.; Ronagh, H. Interlocking System for Enhancing the Integrity of Multi-Story Modular Buildings. *Autom. Constr.* **2018**, *85*, 263–272. [CrossRef]
9. Yang, C.; Xu, Y.C.; Ou, J.P. The frame structure and seismic performance analysis of column-column and beam-beam assembled steel module column-column and beam-beam combined structures. *Seism. Eng. Eng. Vib.* **2022**, *42*, 34–45.
10. Xu, B.; Xia, J.; Chang, H.; Ma, R.; Zhang, L. A Comprehensive Experimental-Numerical Investigation on the Bending Response of Laminated Double Channel Beams in Modular Buildings. *Eng. Struct.* **2019**, *200*, 109737. [CrossRef]
11. An, Q.; Wang, Y.; Wang, X. Study on the load capacity of self-locking cooperative force column of steel structure in modular building. *Ind. Build.* **2023**, 1–13. Available online: https://kns.cnki.net/kcms/detail/11.2068.TU.20230411.1319.002.html (accessed on 3 June 2023). (In Chinese).
12. Qi, A.; Yan, W. Module Building Steel Structure Column Lateral Connection Node and Module Building Steel Structure. CN202122127830.9, 3 September 2021. (In Chinese).
13. *GB 50017-2017*; Standard for Design of Steel Structures. China Architecture & Building Press: Beijing, China, 2017. (In Chinese)
14. Feng, P.; Qiang, H.; Ye, L. The definition and discussion of the "yield point" of materials, components, and structures. *Eng. Mech.* **2017**, *34*, 36–46.
15. *GB 50011-2010*; Code for Seismic Design of Buildings. China Architecture & Building Press: Beijing, China, 2010. (In Chinese)

16. *GB 50009-2012*; Load Code for the Design of Building Structures. China Architecture & Building Press: Beijing, China, 2012. (In Chinese)
17. Chen, R.; Qiu, C.; Hao, D. Design and analysis of multi-story steel structure module. *Build. Struct.* **2019**, *49*, 59–64+18. (In Chinese)
18. *T/CECS 507-2018*; Technical Specification for Steel Modular Buildings. China Planning Press: Beijing, China, 2018. (In Chinese)
19. Charmpis, D.C.; Komodromos, P.; Phocas, M.C. Optimized earthquake response of multi-storey buildings with seismic isolation at various elevations. *Earthq. Eng. Struct. Dyn.* **2012**, *41*, 2289–2310. [CrossRef]
20. Forcellini, D.; Kalfas, K.N. Inter-story seismic isolation for high-rise buildings. *Eng. Struct.* **2023**, *275*, 115175. [CrossRef]
21. Kiani, K.; Nikkhoo, A.; Mehri, B. Parametric analyses of multispan viscoelastic shear deformable beams under excitation of a moving mass. *J. Vib. Acoust.* **2009**, *131*, 051009. [CrossRef]
22. Kiani, K.; Nikkhoo, A.; Mehri, B. Assessing dynamic response of multispan viscoelastic thin beams under a moving mass via generalized moving least square method. *Acta Mech. Sin.* **2010**, *26*, 721–733. [CrossRef]
23. Kiani, K. Axial buckling analysis of vertically aligned ensembles of single-walled carbon nanotubes using nonlocal discrete and continuous models. *Acta Mech.* **2014**, *225*, 3569–3589. [CrossRef]
24. Kiani, K. Nonlocal free dynamic analysis of periodic arrays of single-walled carbon nanotubes in the presence of longitudinal thermal and magnetic fields. *Comput. Math. Appl.* **2018**, *75*, 3849–3872. [CrossRef]